Preprints of the 21st IFAC World Congress (Virtual)
Berlin, Germany, July 12-17, 2020

Novel motorization axis for a Coarse Pointing Assembly in Optical Communication Systems

Lukas Kramer * **Joost Peters** * **Robbert Voorhoeve** *
Gert Witvoet *,** **Stefan Kuiper** *

* *TNO, Dept. of Optomechatronics, Delft, The Netherlands (e-mail: lukas.kramer@tno.nl).*
** *Eindhoven University of Technology, Dept. of Mechanical Engineering, Eindhoven, The Netherlands (e-mail: g.witvoet@tue.nl)*

Abstract: The demand for higher data transfer between satellites and ground stations is ever increasing. To address this, (free-space) optical communication (OC) technology is emerging. Pointing mechanisms with low size, weight and power (SWaP), high accuracy and low recurring costs are key enablers for constellations of OC systems. In this paper, TNO presents a novel motorization concept for coarse pointing assemblies (CPA) using a switched reluctance actuation principle combined with a magnetic hall sensor. Results on a single axis test setup show promising performance in terms of sensor accuracy, pointing jitter and motor control. The presented concept is a potential enabler for future motorization of CPAs.

Keywords: Optical Communication, Pointing Mechanisms, Optomechatronics, Switched Reluctance Motor, Hall Effect Sensor, Linearization, Feedback Control.

1. INTRODUCTION

Scientific and technological developments in the recent decennia have led to an increasing demand in data transfer between satellites and earth. Scientific discovery, e.g. earth observation or the Internet of Things (IoT) require more data and higher data rates. To enable the next steps in high throughput and secure data communication, currently significant progress is being made in the development of optical communication (OC) systems. In contrast to the established method of data communication through radio frequency (RF), in these systems optical sources (lasers) are used. Communication links can range from ground-to-Lower Earth Orbit (LEO, 2000 km) links, to intersatellite (e.g. LEO-to-LEO) links or ground-to-geostationary orbit (GEO, 36000 km) links. Feasibility of optical communication over these links has readily been shown, e.g. in Tolker-Nielsen and Oppenhaeuser (2002), Cazaubiel et al. (2006), Saathof et al. (2019b).

Towards realization of large OC constellations and the required communication terminals, it will be key to develop low cost communication terminals with minimal complexity that can be produced in high volume. Requirements such as low size, weight and power (SWaP), low recurring costs and high reliability form key development drivers. Therefore, TNO (Netherlands Organization for Applied Scientific Research) is developing, together with many industrial partners, OC systems that are reliable, secure and cost effective for ground- and space-based applications. TNO focuses on the design of both complete OC terminals, as well as the development of pointing mechanisms and sensors that are required for these systems (Saathof et al. (2019a,c)).

Communication over large distances using a laser beam requires stringent (a few μrad) pointing performance. Typically, this is achieved by combining a coarse and fine optical pointing mechanism. The fine stage achieves high-bandwidth disturbance rejection with a relatively short stroke (typically a few deg maximum). The Coarse Pointing Assembly (CPA) provides the long stroke pointing of the OC system. Furthermore, it is desired that the CPA does not induce disturbances into the optical path that contains significant power at high frequencies i.e. it is desired to have low positioning jitter. In Kuiper et al. (2018), Witvoet et al. (2018), TNO proposes a low SWaP high performance Fine Steering Mechanism (FSM), that addresses the challenges described in this paragraph for a short stroke mechanism. However, for the coarse stage such low SWaP mechanism with minimal pointing jitter and accurate pointing knowledge is not available. In Mussett et al. (2003), a CPA for OC systems is proposed that uses an open-loop stepper motor with gear-box reduction. In Barbo and Schmid (2003), Szekely et al. (2010) a CPA design is proposed that uses a high end optical encoder combined with a brushless DC motor actuation. Although in these works various designs are proposed for a CPA, in this work the focus is emphasized on a design aiming for low SWaP and costs with smooth tracking behavior based on a different design philosophy.

Therefore, the main contribution of this paper is the development and verification of a novel motorization axis for Coarse Pointing Assemblies based on a switched reluctance motor principle and Hall sensor. The paper is organized as follows. First, in section 2 a design description is provided for the motorization axis. This includes the switched reluctance motor, the magnetic Hall sensor together with

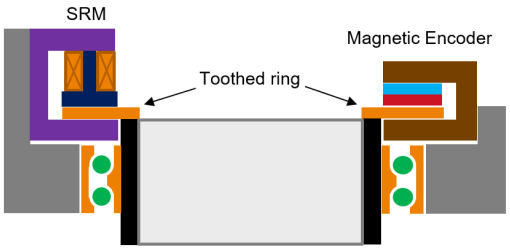

(a) Cross section

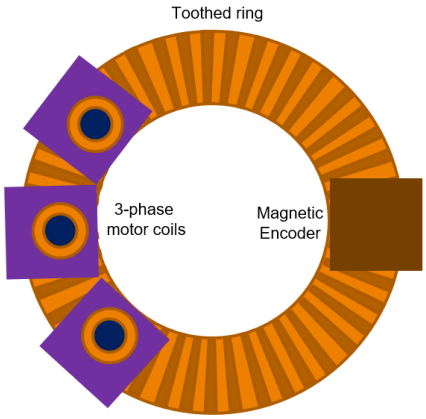

(b) Top view

Fig. 1. Conceptual layout of a CPA motorization axis with SRM, Magnetic Encoder, toothed ring and bearings.

the calibration algorithm. Furthermore, input-output linearization and feedback design is proposed for the control of the motorization axis. In section 3, first results of the single axis test-setup are presented. Finally in section 4 the paper is concluded.

2. DESIGN DESCRIPTION

2.1 Concept description

As introduced in the previous section, the main design drivers for a high volume CPA concept are low SWaP (size, weight and power), low recurring costs, scalability and smooth pointing behavior. To achieve these goals, TNO has developed a novel motorization axis that includes the following features:

- Switched Reluctance Motor (SRM)
- Magnetic Hall encoder
- Soft preloaded bearings

A cross section and top view of the conceptual layout of the novel motorization axis is shown in Fig. 1. The actuation and sensing are combined in a single toothed ring to reduce mass, complexity and costs. The Switched Reluctance Motor (SRM) is a high force density direct drive motor, without wear and low mechanical complexity. The Magnetic encoder is based on a low-cost and space proven Hall sensor chip that measures the magnetic field variations induced by the toothed ring. The static magnetic field offset is created by a permanent magnet. The bearings are preloaded with a soft spring to achieve stable friction behavior resulting in minimal wear and pointing jitter. The motorization concept is easily scalable for different sizes

Table 1. Typical requirements for a LEO-LEO CPA.

Specification	**Value**
Optical aperture	$\varnothing 70$ mm
Range	$\pm 180°$ Azimuth $\pm 20°$ Elevation
Pointing knowledge	< 500 µrad (3σ)
Pointing jitter*	< 1 µrad (3σ)
Power dissipation	< 5 W maximum, < 1 W typical
Mass	< 5 kg

* Jitter is defined as the position error, filtered by the FSM sensitivity function.

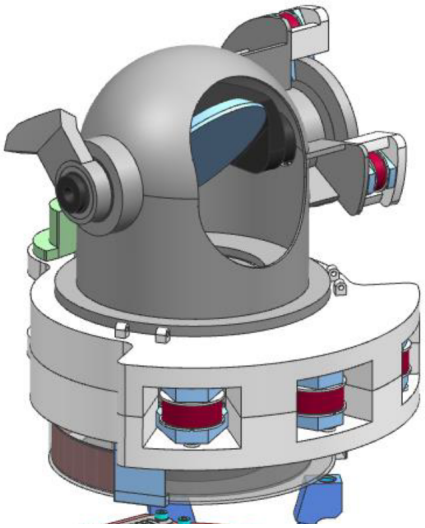

Fig. 2. CAD render of the LEO-LEO CPA design, including the novel motorization axis.

and configurations and can therefore be optimized for each specific application. An integration example of the novel motorization axis in a complete LEO-LEO CPA design is shown in Fig. 2, for which the typical requirements are summarized in table 1. The most important requirements for the motorization axis are the pointing knowledge and jitter. The pointing knowledge is determined by the accuracy of the Hall encoder. The pointing jitter is defined as the position error, filtered by the FSM sensitivity function. This is motivated by the aimed dual-stage pointing design of an OC system, as explained in the introduction.

2.2 Switched Reluctance Motor

The Switched Reluctance Motor (SRM) has gained increasing interest in the last decades, due to its simple construction, reliability and many other advantages over other DC or AC machines as described by Miller (2001). This is mainly caused by the advancement in power electronics and digital signal processing, that allows for simplification of the mechanics at the costs of advanced control methods. The SRM design of the motorization axis has no permanent magnets and therefore does not suffer from motor cogging. The motor has three-phases that are mutually shifted by 120°, such that a continuous torque can be generated. When neglecting magnetic saturation, the torque of a single motor phase can be written as

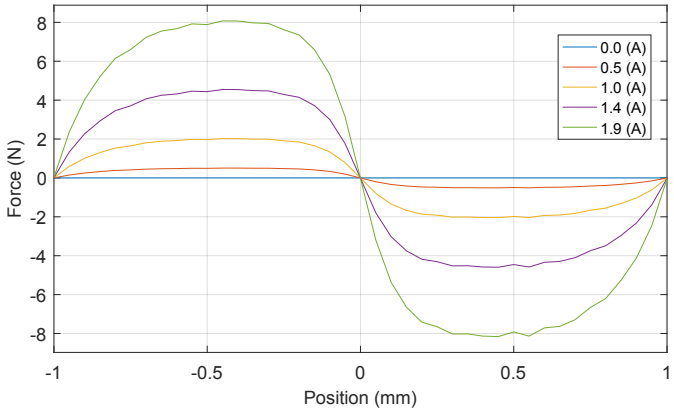

(a) Force of a single motor phase

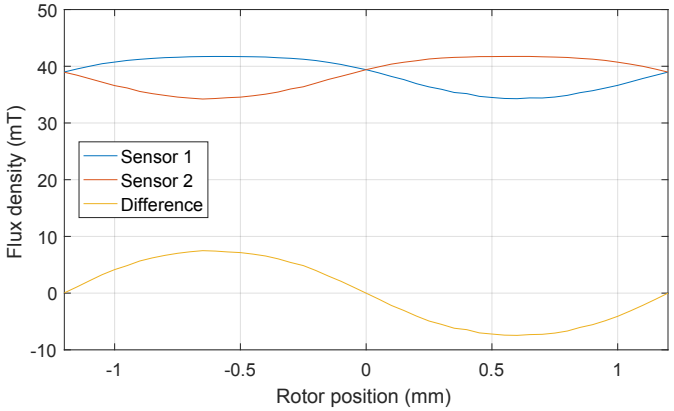

(b) FEM simulation of the Hall encoder

Fig. 3. FEM results for the force of a single motor phase with a limited number of rotor teeth (a) and for Hall sensor 1 and 2 for a static magnetic field of 40 mT (b).

$$T_{\text{phase}} = i_c^2 \underbrace{\frac{1}{2}\frac{\partial L}{\partial \phi_m}}_{G_T(\phi_m)}, \tag{1}$$

where i_c is the coil current and L the inductance of the motor phase, which is determined by the tooth geometry, coil size, magnetic material and the relative motor phase ϕ_m. The motor geometry is designed with first principle analytical modeling and subsequently verified with 2D Finite Element Magnetic Model software. The force generated by a single phase, dependent on current and position, is shown in Fig. 3 (a). The torque of a single phase is the multiplication between force and mean radius of the rotor. The total motor torque, dependent on position, is equal to the summation of the three motor phases that are shifted by a relative phase of 120°.

2.3 Magnetic Hall Encoder

The design drivers for OC system are low SWaP and low complexity. Therefore, in this motorization design a magnetic Hall encoder is used to measure the axis position. Complexity is very limited since the actuation rotor with teeth can be used for sensing as well. The Hall encoder principle is shown in Fig. 4 and consists of four Hall sensors. Sensor 1 & 2 are shifted by 180° relative to the rotor tooth period, which provides the Hall signals in Fig. 3 (b) as obtained with 2D FEM modeling. Subtracting signal

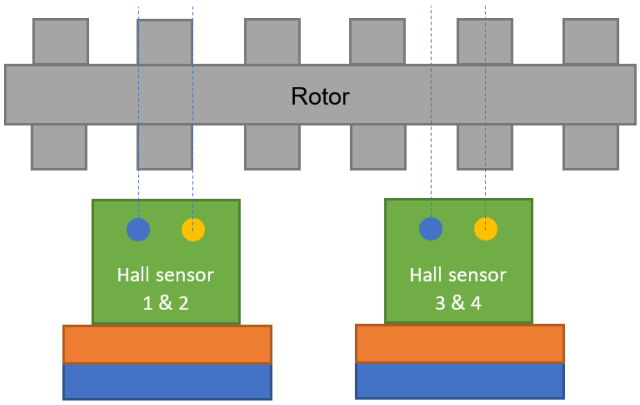

Fig. 4. Working principle of the Hall encoder.

1 & 2 (denoted by s_i) provides a differential measurement of the flux density (d_i), which represents an approximate sine function (depicted in red). By using a second pair of Hall sensor signals, a sin/cos magnetic encoder principle is obtained.

The most straightforward approach to obtain an accurate angular position from the sin/cos encoder signals is to use the 2-argument arctangent, i.e.

$$\theta_z = \text{atan2}(d_1, d_2), \tag{2}$$

where $d_1 = s_1 - s_2$, and $d_2 = s_3 - s_4$ are the differential hall sensor measurements. However, the signals d_1, d_2, are not exact sine or cosine functions. Therefore, θ_z is not equal to the actual angular position denoted by ϕ_z. Furthermore, slight variations in the teeth due to production tolerances will result in variations in the measured flux density. Therefore, a calibration algorithm using an external calibration encoder is formulated to compensate for both rotor teeth variations and higher order terms in the sine/cosine signals. To obtain this, a compensation function is fitted using the calibration encoder based on the following minimization,

$$\hat{\phi_z} = f(\theta_z, i, c_1 \ldots c_N)\,, \tag{3}$$

$$c_1 \ldots c_N = \underset{c_1 \ldots c_N}{\text{argmin}} \, ||f(\theta_z, i, c_1 \ldots c_N) - \phi_z||_2^2, \tag{4}$$

where f can be defined as, e.g., a piecewise polynomial function or a sum of sines, and where a single set of parameters, $c_1 \ldots c_N$, can be determined for all teeth on the rotor, or a different set of parameters can be determined for each i'th tooth on the rotor. Here, ϕ_z is the output of the external calibration encoder (which is not space-compatible and low SWaP). Results of the proposed sensor and calibration algorithm are presented in section 3.

2.4 Control

This section presents the controller design for the motorization axis. The best pointing performance can be achieved when the motor is controlled as a direct drive motor and not as a stepper motor. To this end the commutation algorithm is explained that linearizes the input-output behavior of the SRM, such that classical linear feed-

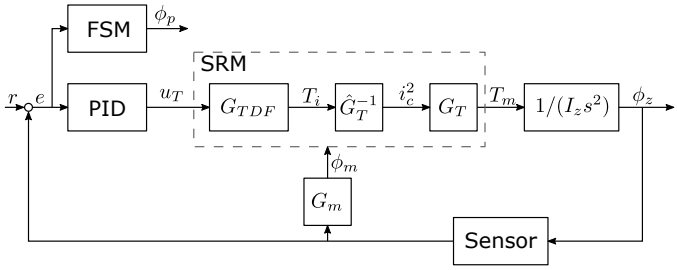

Fig. 5. Control diagram of the motorization axis with PID controller, commutation strategy of the SRM and rotational inertia of the axis.

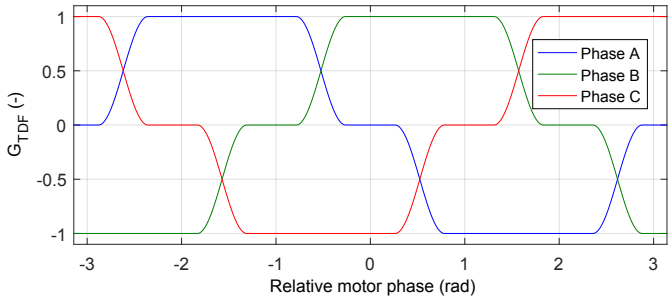

Fig. 6. Torque distribution function G_{TDF} of the different phases as function of relative motor phase (ϕ_m).

back control can be applied. Next, the feedback controller design and considerations are discussed.

Commutation Algorithm The output motor torque is highly non-linear, caused by the position dependency and the quadratic influence of current in (1). The non-linear behavior of the SRM is linearized by the commutation algorithm. The working principle of the SRM with commutation algorithm is shown in Fig. 5. The total motor torque, including commutation, can be written as

$$T_m = \sum_{i=A,B,C} u_T \cdot G_{\mathrm{TDF},i}(\phi_m) \cdot \hat{G}_{T,i}^{-1}(\phi_m) \cdot G_{T,i}(\phi_m), \quad (5)$$

where T_m is the output torque, u_T the required torque and G_{TDF} the torque distribution function between the three phases which sums up to 1. G_T is the gain between the current squared and output torque and should be measured to estimate the inverse $\hat{G}_T^{-1}$. The output torque T_m is equal to u_T when $\hat{G}_{T,i}^{-1} G_{T,i} = 1$, i.e. when G_T is exactly measured and the inverse is implemented in the commutation algorithm. In this way the dominant non-linear input-output behavior of the SRM is linearized.
Different torque distribution functions exist to switch between the different phases, which are in general a trade-off between power efficiency and torque ripple (Vujičić (2012)). The best power efficiency is achieved when only the motor phase is used that has the highest torque gain G_T, but this also results in a torque ripple when switching instantaneously between motor phases. Therefore a different, slightly less power efficient, torque distribution function is used as shown in Fig. 6 and described by Vujičić (2012). The torque distribution is a squared sinusoidal function when switching between the phases to enforce smooth pointing performance.

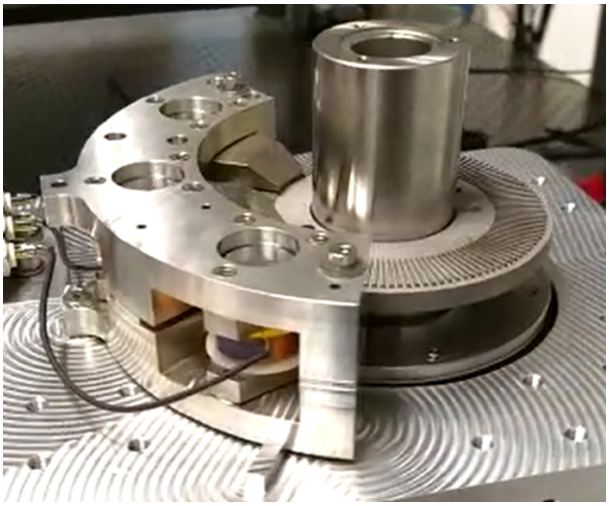

Fig. 7. Photo of the CPA breadboard setup to validate the performance of a single motorization axis.

Controller The pointing performance of the complete system is usually determined by the control bandwidth of the FSM, which is typically a few hundred Hz. The control bandwidth of the CPA is much lower compared to the bandwidth of the FSM and follows from a trade-off between tracking performance for coarse positioning (e.g. to keep the FSM within range) and sensor noise propagation. The frequency content of the CPA error should be as low as possible, such that it can be compensated by the FSM. The bandwidth for the motorization axis is set to 15 Hz, but can be increased or decreased, depending on the error propagation in the system. The controller is a simple PID controller, i.e.:

$$C(s) = k \cdot \left(1 + \frac{2\pi 1.5}{s}\right) \cdot \frac{\frac{s}{2\pi 5} + 1}{\frac{s}{2\pi 45} + 1}, \quad (6)$$

where k is such that a bandwidth of 15 Hz is achieved.

3. TEST RESULTS

In the previous sections the concept, motor, sensor and control principles of the motorization axis are introduced. To verify the proposed concepts and performance, a breadboard test setup has been designed and built. The breadboard test setup is shown in Fig. 7 and consists of a single motorization axis with toothed ring, SRM, Hall encoder, soft preloaded bearings and a Renishaw Signum encoder system. In the following subsections the breadboard results for the motor, Hall encoder and tracking performance are shown.

3.1 Motorization

The torque of the motor has been measured with a force probe at different positions in a single motor period for current levels of 0.2-0.8 A (Fig. 8 (a)). Dividing the measured torques by the current squared provides the measured G_T for the three different phases as shown in Fig. 8 (b). The measured G_T is approximately constant until a current of 0.6 A; for higher currents G_T decreases due to magnetic saturation. The measured G_T is fitted with a sum of sines and inverted to obtain $\hat{G}_T^{-1}$ for the commutation

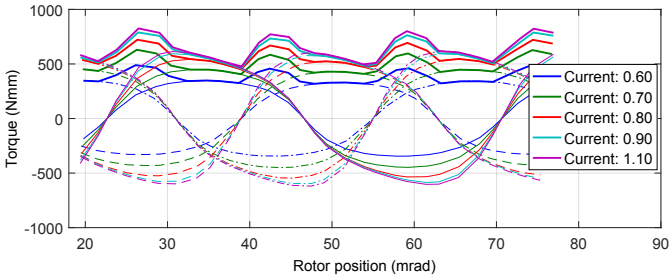

(a) Measured torque

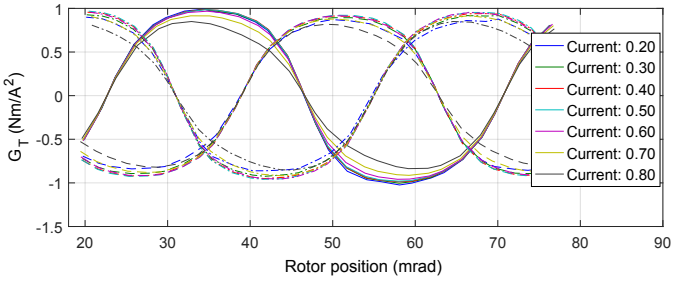

(b) Measured G_T

Fig. 8. Measured phase and total motor torque (a). Dividing the phase torque by the current squared provides G_T for motor phase A, B and C (b).

algorithm, based on current levels until 0.6 A.
The maximum continuous motor torque is between 400 and 500 N mm (Fig. 8 (a)), which is limited by magnetic saturation and the smooth phase transition by the commutation algorithm. For the 500 N mm motor torque, a maximum current of 0.8 A is required (Fig. 8 (b)). To guarantee stability at current levels up to 0.8 A, the gain margin of the controller should be sufficient (typically factor 2). For current levels above 0.8 A, additional measures should be implemented in the commutation algorithm. The difference in motor torque between 2D FEM simulation and measurement of the SRM was found to be within 10%, which indicates that the motor torque can be scaled accurately for each application.

3.2 Hall Encoder

The magnetic field offset of 40 mT for the Hall sensors is generated by a coil, but will be replaced by a small permanent magnet in the final design. The differential Hall signals (d_1 and d_2) provide smooth sinusoidal functions with an amplitude of approximately 5 mT, which corresponds to the 2D FEM simulation in Fig. 3 (b). To verify the performance of the Hall encoder, the calibration algorithm presented in section 2.3 is applied. A polynomial fit is applied to both the *average* measured tooth profile over a full rotation, as well as a piecewise polynomial fit for each *individual* tooth. The calibration error between the reference encoder and the estimated angle $e_\phi = \hat{\phi}_z - \phi_z$ is evaluated and depicted in Fig. 9. It is observed that with the average fit, variation of the specific tooth w.r.t. the average leads to a calibration error. With the piecewise polynomial applied for each individual tooth, it is observed that this is mitigated and thereby making the calibration robust for the expected manufacturing tolerances. Note that this requires an absolute reference on the rotor. Results of the Hall sensor measurements indicate that

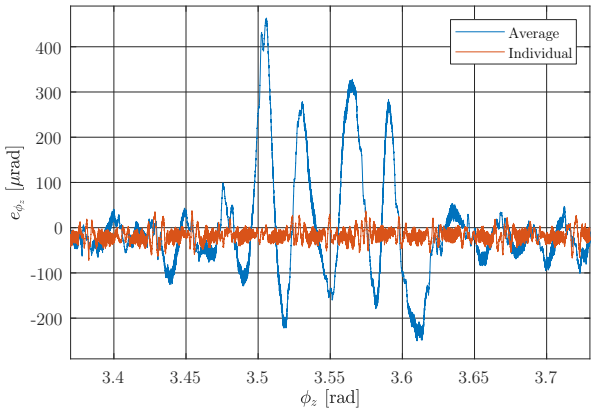

Fig. 9. Results of $e_\phi = \hat{\phi}_z - \phi_z$ for an average tooth fit and a piecewise polynomial fit for each individual tooth.

< 100 µrad can be achieved with the proposed design. Future work includes improving the calibration algorithm for possible sensor/axis drift and feedback control on the Hall encoder.

3.3 System identification

An initial PID controller has been designed based on parameters of the CAD model and implemented in the digital controller. The real plant dynamics have been identified using closed loop system identification at different positions in a single motor period (Fig. 10). The results show that the identified plant dynamics are approximately independent on motor position. This shows that the commutation strategy results in a position independent torque level, as required. The measured slope between 8 and 500 Hz is not identical to a typical mass/inertia line of -40 dB/decade, which is caused by eddy currents in the magnetic material. The constant gain at frequencies below 8 Hz is expected to be caused by the bearing pretension and lubricant. The small resonances at 40 and 80 Hz show small mass decoupling (anti-resonance, resonance), which do not cause instability. The measured plant dynamics are used to update the controller to the required bandwidth.

3.4 Tracking performance

The tracking performance of the motorization axis is measured with the presented SRM, commutation algorithm, controller and Renishaw reference encoder (Renishaw REXM20USA052 i.c.w. SIGNUM SR050A readhead) as feedback sensor. The reference was set to a constant speed of 1 mrad/s, which is the maximum speed of a typical LEO-LEO reference motion with 60° amplitude and a period of 90 minutes. The Power Spectral Density (PSD) of the error is shown in Fig. 11. The tracking error is smaller than 4 µrad rms and dominated by frequency content below 10 Hz. As explained in section 2 and visualized by the pointing variable ϕ_p in Fig. 5, the pointing performance of a complete OC terminal is determined by the combination between a FSM and CPA. As introduced previously, the pointing jitter is defined as the CPA tracking error, filtered by the FSM sensitivity function, which is approximated by a first-order 200 Hz high-pass filter (Witvoet et al. (2018)). The resulting pointing jitter is below 0.3 µrad rms. This is

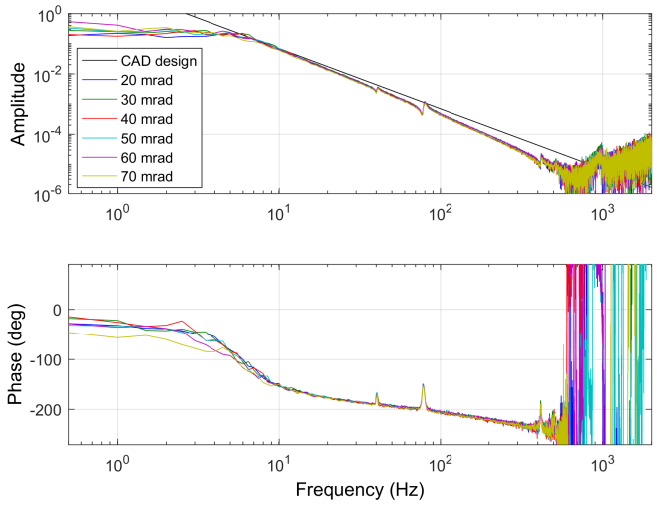

Fig. 10. Measured plant at different rotor positions within one motor period (20 to 70 mrad).

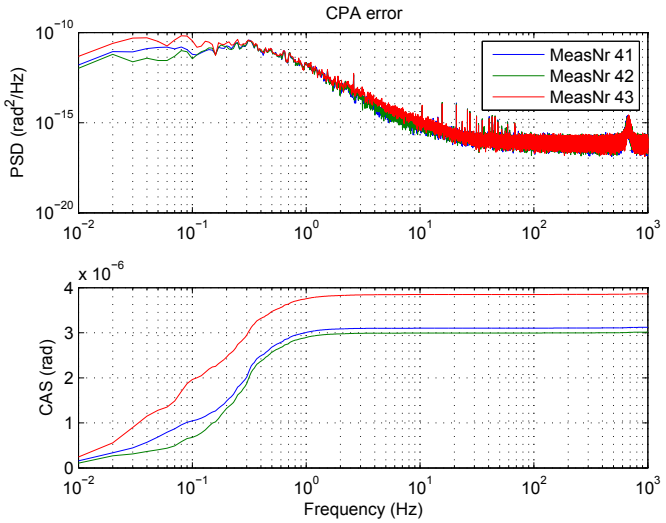

Fig. 11. PSD of the unfiltered CPA error with a 15 Hz bandwidth PID controller.

already within the required pointing jitter specification of 1 µrad (3σ), but note that the filtered error is dominated by high frequency noise of the Renishaw encoder, which is unlikely to be physical axis movement.

4. CONCLUSIONS

In this paper the development and verification of a novel motorization axis for Coarse Pointing Assemblies is presented, where the design has been aimed at low costs and low size, weight and power (SWaP). Results show that with a low SWaP design promising performance has been achieved, enabling a low cost coarse pointing solution for future data communication constellations. The test results show that the measured SRM torque is within 10% of the FEM simulations and therefore indicates that the design could be easily scaled for each specific application. Results of the Hall sensor measurements indicate that an accuracy below 100 µrad can be achieved with the proposed sensor design and calibration. The tracking error is below 4 µrad and reduces below the desired performance of 1 µrad (3σ) when combined with a fine pointing mechanism.
Next steps include further development of the Hall encoder calibration and closed loop control with the Hall encoder as feedback sensor.

ACKNOWLEDGEMENTS

The authors would like to thank the project team-members Martin Siegl, Hans Spierdijk, Bastiaan Oostdijck, Jan de Vreugd, Thijs Moens, Kristiaan Broekens and Andrey Khorev for their valuable contributions to the project.

REFERENCES

Barbo, R. and Schmid, M. (2003). Coarse pointing and fine pointing mechanism (cpa and fpa) for an optical communication link. *Proceedings of the 10th European Space Mechanisms and Tribology Symposium*, 524, 89–96.

Cazaubiel, V., Planche, G., Chorvalli, V., Le Hors, L., et al. (2006). Lola: A 40000 km optical link between an aircraft and a geostationary satellite. In *Sixth International Conference on Space Optics, Proceedings of ESA/CNES ICSO 2006*. ICSO.

Kuiper, S., Doelman, N., Human, J., et al. (2018). Advances of tno's electromagnetic deformable mirror development. In *Proc. SPIE 1070618, Advances in Optical and Mechanical Technologies for Telescopes and Instrumentation III*. SPIE.

Miller, T. (2001). *Electronic Control of Switched Reluctance Machines*. Newnes.

Mussett, D., Humphries, M., Henzelin, F., and Székely, G. (2003). Contraves optical terminal - coarse pointing assembly (cpa). *Proceedings of the 10th European Space Mechanisms and Tribology Symposium*, 524, 81–88.

Saathof, R., Crowcombe, W., Kuiper, S., et al. (2019a). Optical satellite communication space terminal technology at tno. In *Proc. International Conference on Space Optics*. SPIE.

Saathof, R., den Breege, R., Klop, W., Doelman, N., et al. (2019b). Pre-correction adaptive optics performance for a 10 km laser link. In *Proc. SPIE 10910, Free-Space Laser Communications XXXI*. SPIE.

Saathof, R., Kuiper, S., Crowcombe, W., de Man, H., and de Lange, D. (2019c). Opto-mechatronics system development for future intersatellite laser communications. In *Proc. SPIE 10910, Free-Space Laser Communications XXXI*. SPIE.

Szekely, G., Blum, D., Humphries, M., Koller, A., et al. (2010). A coarse pointing assembly for optical communication. In *Proceedings of the 40th Aerospace Mechanisms Symposium*. NASA.

Tolker-Nielsen, T. and Oppenhaeuser, G. (2002). In-orbit test result of an operational optical intersatellite link between artemis and spot4, silex. In *Proceedings of SPIE*, 973902. SPIE.

Vujičić, V. (2012). Minimization of torque ripple and copper losses in switched reluctance drive. *IEEE Transactions on Power Electronics*, 27(1), 388–399.

Witvoet, G., Kuiper, S., and Meskers, A. (2018). Performance validation of a high-bandwidth fine steering mirror for optical communications. In *Proc. of SPIE 11180,, International Conference on Space Optics*, volume 11180. SPIE.